

Electroweak corrections to W-boson pair production at the LHC

ANASTASIYA BIERWEILER¹, TOBIAS KASPRZIK¹, JOHANN H. KÜHN¹,
SANDRO UCCIRATI²

¹*Karlsruhe Institute of Technology (KIT), Institut für Theoretische Teilchenphysik,
D-76128 Karlsruhe, Germany*

²*Universität Würzburg, Institut für Theoretische Physik und Astrophysik,
D-97074 Würzburg, Germany*

Abstract:

Vector-boson pair production ranks among the most important Standard-Model benchmark processes at the LHC, not only in view of on-going Higgs analyses. These processes may also help to gain a deeper understanding of the electroweak interaction in general, and to test the validity of the Standard Model at highest energies. In this work, the first calculation of the full one-loop electroweak corrections to on-shell W-boson pair production at hadron colliders is presented. We discuss the impact of the corrections on the total cross section as well as on relevant differential distributions. We observe that corrections due to photon-induced channels can be amazingly large at energies accessible at the LHC, while radiation of additional massive vector bosons does not influence the results significantly.

August 2012

Corresponding author: Tobias Kasprzik (kasprzik@particle.uni-karlsruhe.de)

1 Introduction

With the recent start of LHC operation hard scattering processes became accessible with parton energies up to several TeV and, indeed, jet-jet invariant masses up to 5 TeV have been observed [1, 2] in the first round of data taking. With the significant increase of the integrated luminosity and the doubling of the beam energy anticipated in the next few years, electroweak processes such as the production of lepton or gauge-boson pairs with invariant masses of several TeV will become accessible in the near future. These reactions may on the one hand allow for precise tests of the Standard Model (SM) and on the other hand potential deviations may point to “physics beyond the SM”. Indeed, the observation of anomalous couplings of quarks, leptons or gauge bosons might well be the first signal of “New Physics”. As an alternative one may look for peaks or distortions in the W, Z or fermion spectra resulting from the decays of new massive particles. Clearly, any well-founded claim of “physics beyond the SM” must be based on precise measurements combined with similarly precise calculations, possibly at the level of several percent.

Obviously this requires theory predictions which must include next-to-leading order (NLO), possibly even next-to-next-to-leading order (NNLO) perturbative QCD corrections. Considering the smallness of the weak coupling, α_w , the need for electroweak (EW) corrections is less obvious. In a first step one might try to absorb the dominant corrections arising from the running of the fine-structure constant from low scales to M_Z and from the ρ -parameter [3] in properly chosen effective couplings. However, this approach is only justified for energies of order M_W or M_Z . As is well known from earlier investigations [4–17], EW corrections increase with the squared logarithm of the energy, and may reach several tens of percent for energies accessible at the LHC. In view of their strong dependence both on energy and scattering angle, they will induce significant distortions in transverse-momentum and rapidity distributions and consequently may well mimic “New Physics” and hence must be carefully taken into account.

Most of the investigations along these lines have concentrated on the issue of Sudakov logarithms, i.e. terms that are at n loops enhanced proportional to $\alpha_w^n \log^{2n-m}(s/M_W^2)$ with $m = 0, 1, \dots, 2n$, corresponding to leading, next-to-leading etc. logarithmic (N^m LL) enhancement. This line of research was motivated by the necessity of including at least the dominant two-loop terms, once one-loop corrections exceed the 20 – 30% level. Using evolution equations, originally derived in the context of QED [18–21] and QCD, four-fermion processes have been studied up to N^4 LL [7, 11–14], W-pair production in electron–positron and quark–antiquark annihilation up to N^3 LL [22, 23]. Employing diagrammatic methods or the framework of soft-collinear effective field theory most of these results were confirmed in the NLL and NNLL approximation [8, 10, 16, 24].

As stated above, the intermediate energy region, up to approximately 1 TeV, will be explored with high statistics, and the complete one-loop corrections may become relevant. This includes real and virtual photon radiation and terms suppressed by M_W^2/\hat{s} , where \hat{s} denotes the partonic center-of-mass (CM) energy squared. Up to now these complete one-loop corrections have been evaluated for $t\bar{t}$ [25–29] (for earlier studies see [30, 31]), $b\bar{b}$ [32], as well as for gauge-boson plus jet production, the latter in the on-shell approximation [33–38] and including W- or Z-decays to leptons with all off-shell effects consistently taken into account [39, 40].

In contrast, the full one-loop EW corrections to vector-boson pair production at the LHC are not yet available, despite their great phenomenological interest. These processes contribute the most important irreducible background to the production of a SM Higgs boson in the intermediate mass range. A profound theoretical understanding of the underlying physics will also allow a precise analysis of the non-abelian structure of the EW sector, in particular of the vector

boson self interactions. At the LHC these will be explored with high precision, exploiting the high luminosity in combination with the highest possible CM energies. Moreover, vector-boson pair production processes are well suited for putting experimental constraints on the existence of anomalous trilinear and quartic gauge couplings, since their phenomenological effects are expected to be sizable at large invariant masses of the vector-boson pairs accessible at the LHC. Considering searches for supersymmetry (SUSY) at the LHC, all vector-boson pair production channels constitute important backgrounds to signals with leptons and missing transverse energy, as e.g. predicted for chargino–neutralino pair production.

During recent years, a great effort has been made to push the accuracy of the theoretical predictions to a new level. The NLO QCD corrections, including the leptonic decays of the vector bosons, have been studied by several authors and are implemented in Monte Carlo programs [41–49]. The results have been matched with parton showers and combined with soft gluon resummations [50] to improve the predictions for vector bosons produced at small transverse momenta. The loop-induced channels $gg \rightarrow V_1 V_2$, formally a second order effect in QCD, nevertheless play an important role at the LHC due to the enhancement of the gluon luminosity and have also been studied extensively [51–54]. Specifically, concerning background estimates to Higgs production at the LHC, the contribution of the gluon-induced channel to W-boson pair production amounts to 30% after experimental cuts [54].

Electroweak corrections for gauge-boson pair production at hadron colliders, however, have only been evaluated in the high energy limit [55–57]. This is in contrast to the reaction $e^+e^- \rightarrow W^-W^+$, where the complete one-loop calculation has long been available [58–61], and, following the demands of LEP experiments, the full one-loop correction for electron–positron annihilation into four fermions (including resonant and non-resonant amplitudes) has been calculated [62–65].

To arrive at predictions which satisfy the needs of the next round LHC experiments, we embark on the full one-loop corrections for W-pair production in proton–proton collisions, where the gauge bosons are treated as stable particles. For completeness we also recalculate the well-known NLO QCD corrections and, furthermore, discuss two competing processes: W-pair production through $\gamma\gamma$ collisions, and through the quark-loop-induced gluon-fusion process. Employing the MRST2004QED PDF set [66] for the $\gamma\gamma$ luminosity, we observe a surprisingly large contribution at large invariant W-pair mass and a pronounced peaking at small scattering angles. In fact, for small angles and high energies this parametrically suppressed reaction is comparable to the $q\bar{q}$ induced reaction. Even for large angles (i.e. large p_T) it still amounts to order of 5% and is therefore comparable with the genuine EW corrections. Gluon fusion, in contrast, exhibits a fairly smooth angular distribution and is typically of order 5 to 10 percent in the whole kinematic region of interest. Obviously all these effects must be taken into consideration.

The layout of this paper is as follows: In Section 2 we start with a qualitative discussion of W-pair production at leading order (LO). We introduce the kinematic variables and recall the dominant features of W production: the dependence on the W transverse momentum, W-pair invariant mass and rapidity. These results will illustrate the large kinematic region accessible at the LHC and the marked differences between the $q\bar{q}$ -, gg- and $\gamma\gamma$ -induced channels, as far as transverse-momentum and angular distributions are concerned. Section 3 will be devoted to a detailed discussion of one-loop EW corrections to the reaction $q\bar{q} \rightarrow W^-W^+$. We specify the renormalization scheme, our input parameters, the treatment of QED corrections with the associated soft and collinear singularities, their absorption in the PDFs, and the numerical evaluation of hard photon radiation. As stated above the rate of W-pair production from $\gamma\gamma$ collisions is surprisingly large and the resulting rates and distributions are studied in Section 4. The cross sections for $q\bar{q} \rightarrow W^-W^+$ including EW and QCD corrections are convoluted with

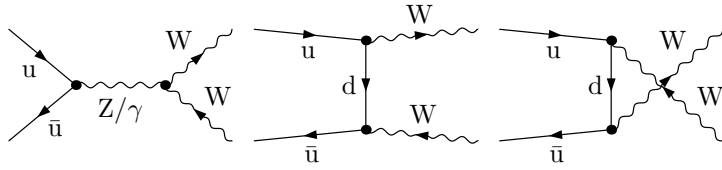


Figure 1: Tree-level diagrams for the LO process $u\bar{u} \rightarrow W^-W^+$.

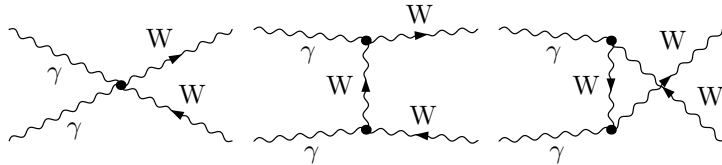


Figure 2: Tree-level diagrams for the LO processes $\gamma\gamma \rightarrow W^-W^+$.

PDFs, and predictions for various distributions are shown and compared with those from $\gamma\gamma$ and gluon-fusion processes. For future tests and cross checks tables are presented which precisely specify the results at various kinematic points. In Section 5, we discuss the phenomenological impact of additional massive vector bosons in the final state. Section 6 contains our conclusions.

2 W-pair production: the leading order

At lowest order, $\mathcal{O}(\alpha^2)$, W-boson pair production at the LHC is dominated by quark–antiquark annihilation,

$$q_i\bar{q}_j \rightarrow W^-W^+, \quad (2.1)$$

where the q_k denote one of the light quark flavours, $q_k = u, d, s, c$ and b . The corresponding diagrams are shown in Fig. 1 for the $u\bar{u}$ channel. Since there is a finite probability of finding a photon in a proton we in addition take into account the photon-induced tree-level contributions

$$\gamma\gamma \rightarrow W^-W^+ \quad (2.2)$$

(see Fig. 2). In the numerical analysis the MRST2004QED PDF set [66] is used for the photon density. Although suppressed by two photon-PDF factors, this channel may give rise to potentially large contributions at high invariant masses. For completeness, we also re-calculate the effects due to the loop-induced channel

$$gg \rightarrow W^-W^+, \quad (2.3)$$

which adds a relative correction of about 10% to the LO $q\bar{q}$ cross section [52].

Due to the large CM energies accessible at the Tevatron and the LHC, we can safely neglect the lepton and light quark masses (i.e. all but the top-quark mass) unless they are needed to regularize infrared (IR) singularities in the real and virtual contributions, as will be discussed later. However, the $b\bar{b}$ channel receives contributions from top-quark exchange in the t channel that for consistency have to be taken into account in the Born approximation and in the NLO calculation. In this work we assume a block-diagonal CKM matrix with $V_{tb} = 1$. Therefore, the

cross sections (2.1) are proportional to $\sum_{k=1}^2 V_{ik} V_{kj}^* = \delta_{ij}$ for $i, j = 1, 2$, and it is sufficient to only consider flavour-diagonal processes. Consequently, at the parton level the complete one-loop calculation has to be carried out independently for the following three different channels,

$$u \bar{u} \rightarrow W^- W^+, \quad (2.4a)$$

$$d \bar{d} \rightarrow W^- W^+, \quad (2.4b)$$

$$b \bar{b} \rightarrow W^- W^+. \quad (2.4c)$$

Let us, in a first step, evaluate the LO prediction for $q\bar{q}$ -, $\gamma\gamma$ - and gg -induced processes. The cross sections for W -pairs as a function of p_T^{cut} , corresponding to a cut on the transverse momenta of the W bosons, and as a function of M_{WW}^{cut} , corresponding to a cut on the mass of the W -pair, are shown in Figs. 3 and 4, respectively. The input values and setup we use for our computation will be specified in Section 4.1, together with the rapidity and p_T cuts employed throughout. Given an integrated luminosity of 20 fb^{-1} at 8 TeV and 200 fb^{-1} at 14 TeV, transverse momenta (invariant masses) up to 0.35 TeV (1 TeV) can be explored at 8 TeV and up to 0.75 TeV (2 TeV) at 14 TeV. Here, we assume that events with one W boson decaying into $e\nu_e$ or $\mu\nu_\mu$ and one decaying hadronically can be detected with 30% efficiency and require more than 100 detected events.

When comparing the p_T^{cut} and M_{WW}^{cut} dependence of $q\bar{q}$ -, $\gamma\gamma$ - and gg -induced processes, marked differences can be observed. For large M_{WW}^{cut} the rates of $\gamma\gamma$ - and $q\bar{q}$ -induced reactions are quite comparable. However, the cut on p_T reduces the relative effect of the photon-induced channels significantly. This is shown on the right hand sides of the respective figures, where the cross sections of the gg - and $\gamma\gamma$ -induced reactions relative to the $q\bar{q}$ -induced process (denoted as δ_{gg} and $\delta_{\gamma\gamma}$, respectively) are plotted. Let us first concentrate on the LHC at 14 TeV (LHC14). The relative rate for W -pairs from gluon fusion amounts to less than 10% for small p_T and decreases with increasing p_T (Fig. 3). The parametric suppression of $gg \rightarrow W^- W^+$ by α_s^2 is compensated by the large gluon luminosity for small $\tau = \hat{s}/s$ which, however, dies out with increasing τ . A qualitatively similar behaviour is observed for a cut on M_{WW} (Fig. 4). The relative importance of the photon-induced process, in contrast, increases with increasing p_T^{cut} , and even more so with M_{WW}^{cut} . This behaviour can be traced to the energy dependence of the cross section for the partonic subprocess $\gamma\gamma \rightarrow W^- W^+$, which approaches a constant value in the high-energy limit, $\hat{\sigma}_{\gamma\gamma} \approx 8\pi\alpha^2/M_W^2$, with an extremely strong peaking in the forward and backward directions. The cut on p_T , when compared to the one on M_{WW} thus leads to a significantly stronger reduction of the event rate. Nevertheless, a 10% admixture of photon-induced W -pairs remains for p_T above 800 GeV. Qualitatively similar statements are applicable to the LHC at 8 TeV (LHC8). However, the relative contributions of both gg - and $\gamma\gamma$ -induced reactions are significantly smaller, and become completely negligible for the Tevatron. In the right three plots of Figs. 3 and 4 we also anticipate some of the results on one-loop QCD (δ_{QCD}) and EW (δ_{EW}) corrections. For transverse momenta around 800 GeV, accessible at LHC14, large negative EW corrections amount to nearly -50% and are the main subject of this paper. In fact, they are quite comparable to the positive QCD corrections, which are displayed in the same figures. Note that the latter strongly depend on the cuts on real jet radiation, as will be discussed at the end of Section 3.3.

As indicated above, the difference between the p_T^{cut} and M_{WW}^{cut} dependence of the cross sections can be traced to the different angular distributions of the W bosons in the W -pair rest frame, which for $\gamma\gamma$ is strongly peaked in the forward and backward directions. The marked differences in the angular distributions are illustrated in Fig. 5, where the distributions in the rapidity difference $\Delta y_{WW} = y_{W^-} - y_{W^+}$ (which, for fixed M_{WW} , corresponds to the angular distribution in the W -pair rest frame) are shown for the mass intervals $[2M_W, \infty]$ and $[1000 \text{ GeV}, \infty]$, respectively.

In the first case, the cross section is dominated by central events with W-pairs of low invariant mass and relatively isotropic angular distributions. All three components are peaked at small Δy_{WW} . Considering their ratios, displayed on the r.h.s. one observes the stronger preference of the gg process for small Δy_{WW} and, conversely, the enhancement of the $\gamma\gamma$ process for large Δy_{WW} . Considering events with large invariant mass, $M_{\text{WW}} > 1$ TeV, the distribution of the three components exhibits a drastically different behaviour. The rate of the gluon-fusion process is fairly small and its angular distribution does not exhibit any pronounced structure, resulting in a flat rapidity distribution. As expected, W-pair production is dominated by $q\bar{q}$ annihilation with its strong peaking at small \hat{t} , i.e. in the forward and backward directions. This is reflected in the peaks of Δy_{WW} around ± 2.5 . The contribution from $\gamma\gamma$ fusion remains sizable, with a very pronounced peaking for large rapidity difference, corresponding to a highly anisotropic angular distribution in the WW rest frame. The EW corrections exhibit a completely different behaviour. For large Δy_{WW} , corresponding to small \hat{t} they are negative but less than 10%. In the Sudakov regime, however, corresponding to small Δy_{WW} and thus large \hat{t} , the Sudakov effect comes into play and negative corrections of more than 30% are observed. In total, the sum of these corrections, denoted $\Sigma\delta$ in the right displays of Fig. 5, will lead to a dramatic distortion of $d\sigma/d\Delta y_{\text{WW}}$ with corrections varying between +30% and -30% for large and small $|\Delta y_{\text{WW}}|$, respectively. Note that such a behaviour could well be misinterpreted as a signal for anomalous couplings.¹ A less pronounced, but qualitatively similar behaviour is observed for LHC8 with the mass intervals $[2M_{\text{W}}, \infty]$ and $[500 \text{ GeV}, \infty]$ (Fig. 6).

3 Radiative corrections

In addition to the tree-level contributions, a full $\mathcal{O}(\alpha^3)$ analysis of the W-boson pair production cross section requires the inclusion of the one-loop EW corrections as well as the contributions due to radiation of one additional bremsstrahlung photon. Thus, the corresponding total partonic cross section at NLO may be written as

$$\hat{\sigma}_{\text{NLO}}^{ij \rightarrow \text{WW}(\gamma)} = \hat{\sigma}_{\text{LO}}^{ij \rightarrow \text{WW}} + \hat{\sigma}_{\text{virt}}^{ij \rightarrow \text{WW}} + \hat{\sigma}_{\text{LO}}^{ij \rightarrow \text{WW}\gamma}, \quad (3.1)$$

with $i, j = u, d, s, c, b, \gamma$ and the corresponding antiparticles, and the different partonic contributions are given by

$$\hat{\sigma}_{\text{LO}}^{ij \rightarrow \text{WW}} + \hat{\sigma}_{\text{virt}}^{ij \rightarrow \text{WW}} = \frac{1}{N_{ij}} \frac{1}{2\hat{s}} \int d\Phi(\text{W}^-\text{W}^+) \sum_{\text{col}} \sum_{\text{spin}} \sum_{\text{pol}} [|\mathcal{M}_0|^2 + 2\text{Re}(\mathcal{M}_0^* \mathcal{M}_1)], \quad (3.2)$$

$$\hat{\sigma}_{\text{LO}}^{ij \rightarrow \text{WW}\gamma} = \frac{1}{N_{ij}} \frac{1}{2\hat{s}} \int d\Phi(\text{W}^-\text{W}^+\gamma) \sum_{\text{col}} \sum_{\text{spin}} \sum_{\text{pol}} |\mathcal{M}_\gamma|^2. \quad (3.3)$$

Here, \mathcal{M}_0 , \mathcal{M}_1 and \mathcal{M}_γ denote the corresponding Feynman amplitudes of the tree-level, one-loop and bremsstrahlung contributions, respectively, $\int d\Phi(\text{final state})$ is the Lorentz invariant phase-space measure of the final-state particles and \hat{s} is the partonic CM energy. The normalization factors are given by $N_{q\bar{q}} = 36$ and $N_{\gamma\gamma} = 4$. Defining the momentum fractions x_a and x_b of the initial-state hadrons carried by the incoming partons, the hadronic NLO cross sections at the

¹The interplay of logarithmic EW corrections and anomalous trilinear gauge-boson couplings has been studied in Ref. [67] for WZ and WW production.

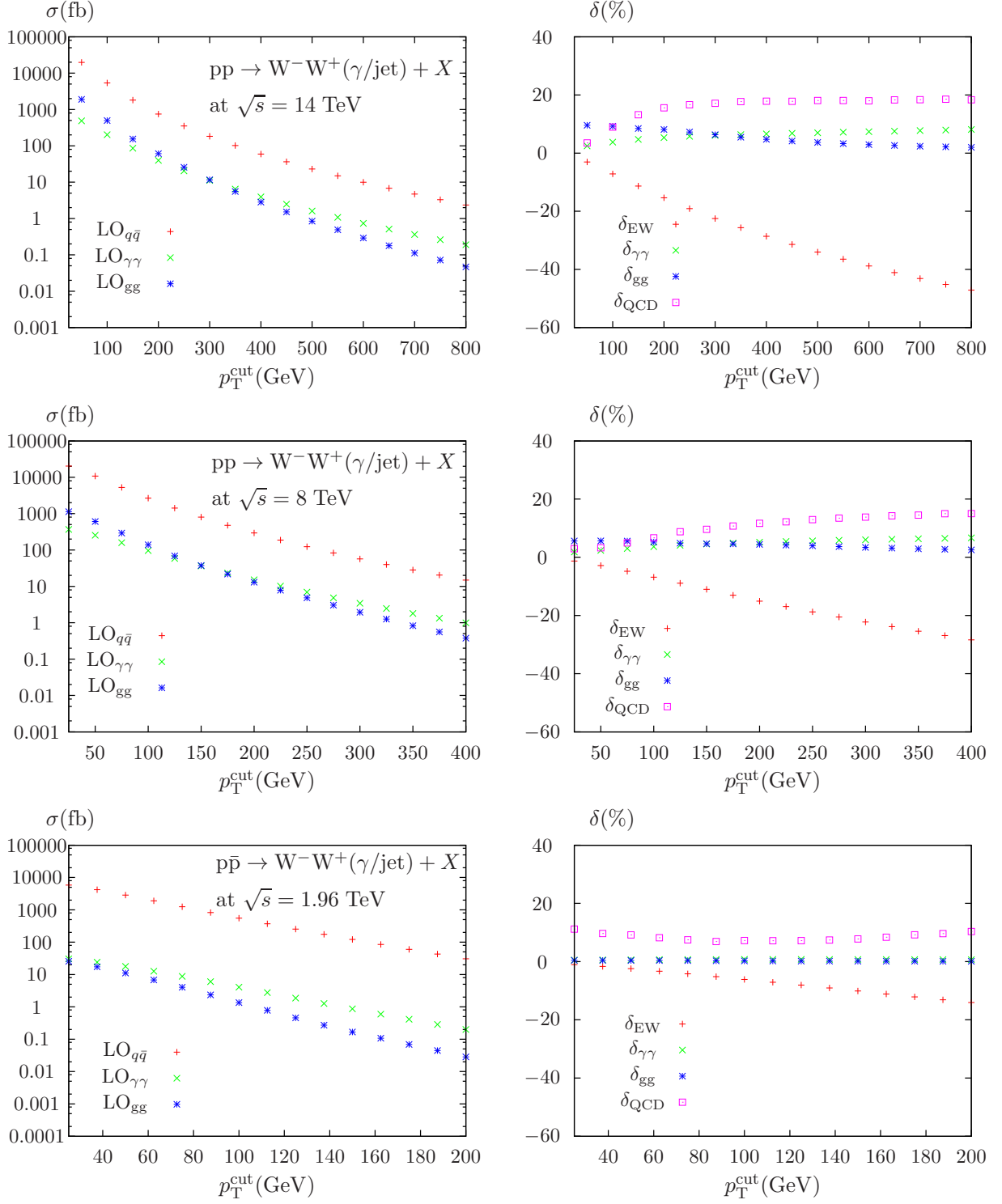


Figure 3: Left: Total cross sections as a function of the cut on the W-boson transverse momentum at the LHC14 (top), LHC8 (center) and the Tevatron (bottom). The corresponding relative rates w.r.t. to the $q\bar{q}$ channel are shown on the r.h.s., together with the rates of QCD and EW corrections. See text for details.

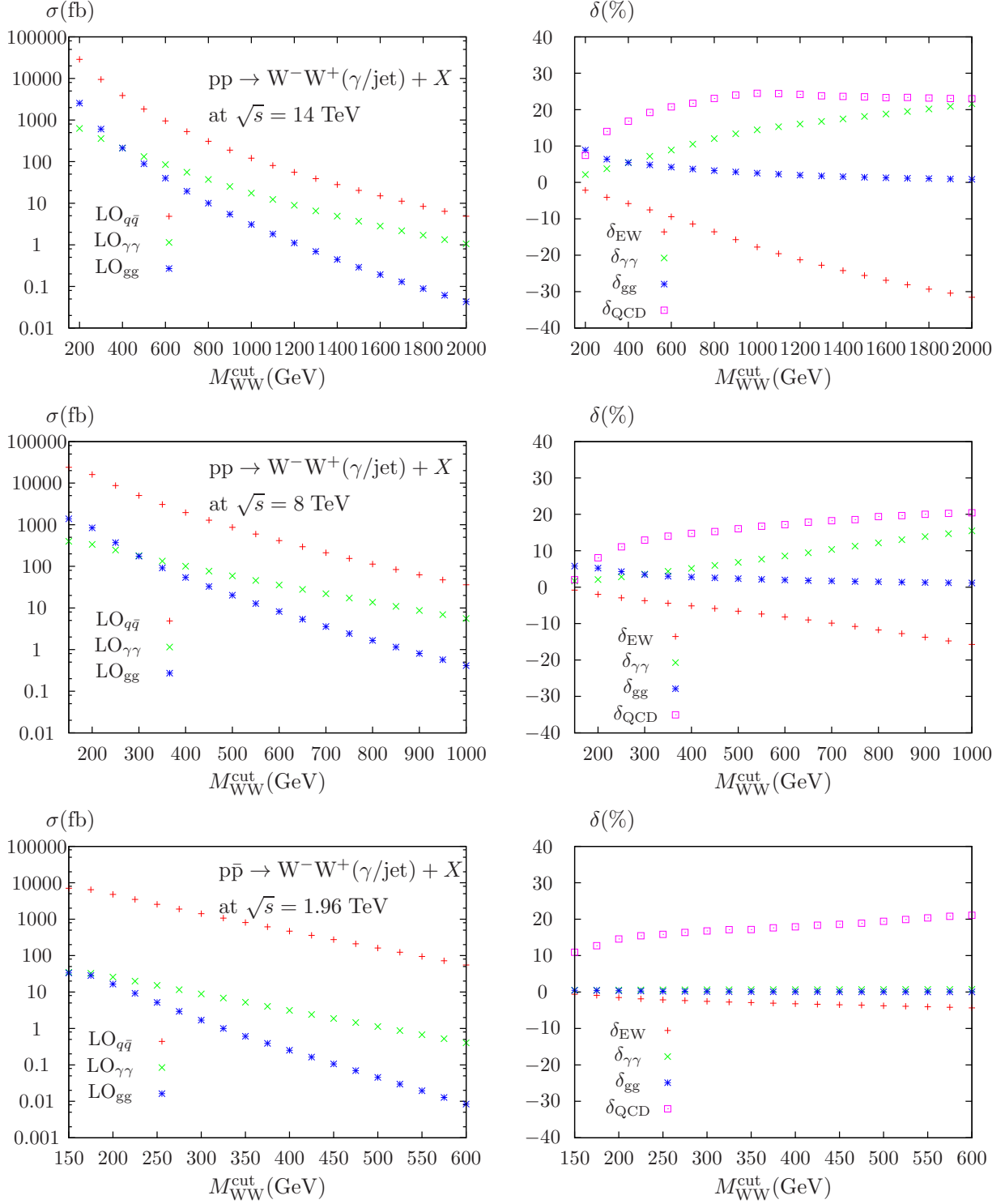


Figure 4: Left: Total cross sections as a function of the cut on the WW-invariant mass at the LHC14 (top), LHC8 (center) and the Tevatron (bottom). The corresponding relative rates w.r.t. to the $q\bar{q}$ channel are shown on the r.h.s., together with the rates of QCD and EW corrections. See text for details.

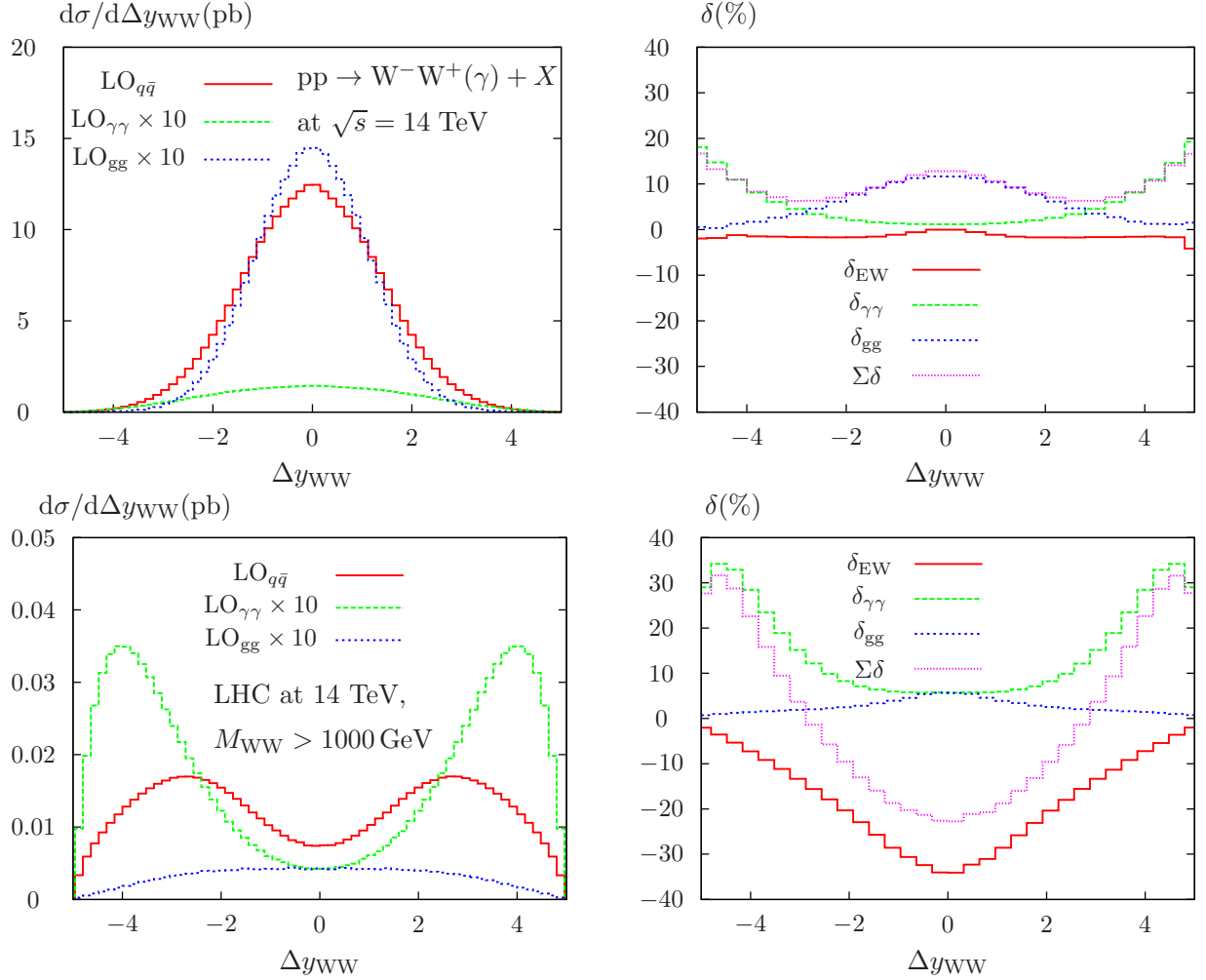


Figure 5: Differential LO cross sections for the W-boson rapidity gap with default cuts (top) and with a minimal invariant mass of 1000 GeV (bottom) at the LHC14. On the right-hand-side, the corresponding relative rates due to photon- and gluon-induced channels w.r.t. the $q\bar{q}$ -contributions are shown, as well as the EW corrections. See text for details.

LHC is given by a convolution of the partonic cross section with the parton distribution functions (PDFs),

$$\sigma_{\text{NLO}}^{\text{pp} \rightarrow \text{WW}(\gamma)} = \int_{\tau_0}^1 d\tau \int_{\tau}^1 \frac{dx_b}{x_b} \sum_{i,j} f_{i/p}(x_a, \mu_{\text{F}}^2) f_{j/p}(x_b, \mu_{\text{F}}^2) \hat{\sigma}_{\text{NLO}}^{ij \rightarrow \text{WW}(\gamma)}(\tau s, \mu_{\text{F}}^2), \quad (3.4)$$

where the hadronic CM energy s is related to \hat{s} via $\hat{s} = \tau s$, with $\tau = x_a x_b$. The kinematic production threshold of a W-boson pair in the final state is reflected in the choice of the lower integration boundary $\tau_0 = 4M_{\text{W}}^2/s$, corresponding to a minimal partonic CM energy of $\hat{s}_0 = \tau_0 s$, and μ_{F} denotes the factorization scale.

We have performed two completely independent calculations of the EW corrections, and the results displayed in Tables 1–4 have been reproduced by both of them.

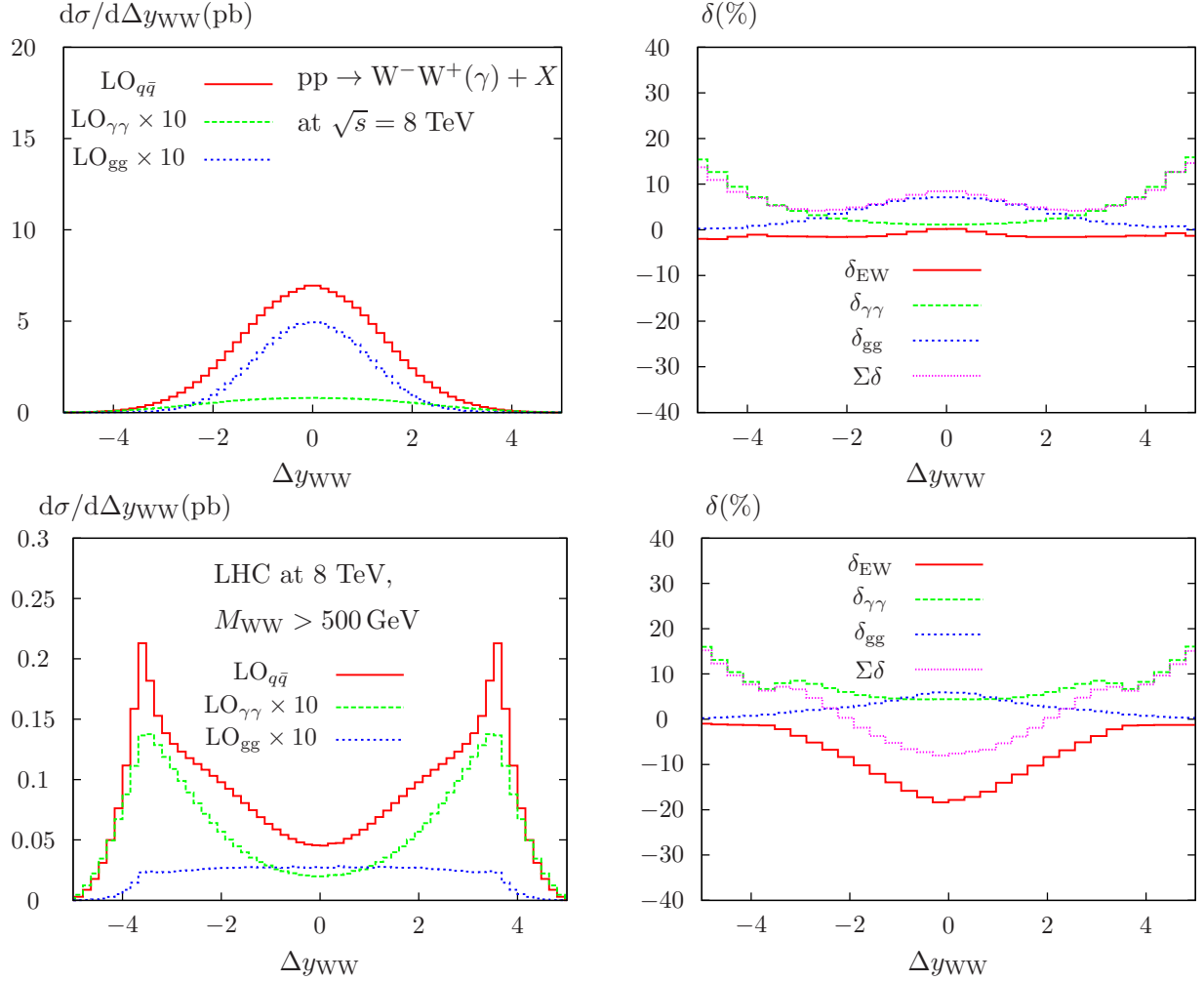


Figure 6: Differential LO cross sections for the W-boson rapidity gap with default cuts (top) and with a minimal invariant mass of 500 GeV (bottom) at the LHC8. On the right-hand-side, the corresponding relative rates due to photon- and gluon-induced channels w.r.t. the $q\bar{q}$ -contributions are shown, as well as the EW corrections. See text for details.

3.1 Virtual corrections and renormalization

The virtual one-loop corrections receive contributions from self-energies, triangles and box diagrams. In the first approach the diagrams are automatically generated with `FeynArts 3.5` [68,69] and `FormCalc 6.1` [70,71] is used to calculate and algebraically simplify the corresponding amplitudes. Afterwards, the multiplication with the Born-level amplitude, as well as the summation (averaging) over polarisations, spins and colours is performed completely analytically within the `FormCalc` framework.

In an alternative approach we used the program `QGraf` [72] to generate Feynman diagrams. The implementation of Feynman rules, the reconstruction of the Dirac structure (as well as the evaluation of Dirac traces) and the calculation of squared matrix elements is carried out analytically using the computer algebra program `FORM` [73]. To avoid numerical instabilities,

potentially small Gram-determinants, which occur in the tensor reduction of particular four-point-functions are cancelled at the analytical level using FORM.

We use two different analytical implementations of the Passarino–Veltman algorithm [74] (based on *Mathematica* and FORM, respectively) to reduce tensor coefficients to scalar integrals. The reduction was also tested against the numerical approach implemented in the `LoopTools 2.5` [70, 75] library, which is used for the evaluation of the scalar one-loop integrals.

The ultraviolet (UV) divergencies that arise in the computation of the one-loop diagrams are treated in dimensional regularization going from 4 to $D = 4 - 2\epsilon$ space-time dimensions, where the UV divergencies appear as single poles in the small complex parameter ϵ . After adding the counterterms in a proper renormalization procedure, the poles vanish, and the limit $\epsilon \rightarrow 0$ can be taken to obtain physical results.

Our results are based on the on-shell renormalization scheme defined in the following.

3.1.1 On-shell scheme

Our choice for the renormalization prescription is the on-shell (OS) renormalization scheme as specified in Ref. [76]. Instead of defining the electromagnetic coupling constant α in the Thomson-limit, however, we work in the G_μ scheme where α is derived from the Fermi-constant G_μ via

$$\alpha_{G_\mu} = \frac{\sqrt{2}G_\mu M_W^2}{\pi} \left(1 - \frac{M_W^2}{M_Z^2} \right). \quad (3.5)$$

In this scheme, the weak corrections to muon decay Δr are included in the charge renormalization constant δZ_e by the replacement

$$\delta Z_e|_{\alpha(0)} \rightarrow \delta Z_e|_{\alpha_{G_\mu}} = \delta Z_e|_{\alpha(0)} - \frac{\Delta r}{2} \quad (3.6)$$

in the calculation of the counterterm contributions (see, e.g., Ref. [77]). As a consequence, the EW corrections are independent of logarithms of the light-quark masses. Moreover, this definition effectively resums the contributions associated with the running of α from zero to the weak scale and absorbs some leading universal corrections $\propto G_\mu m_t^2$ from the ρ parameter into the LO amplitude.

3.2 Real corrections

In a second step, the diagrams contributing to the bremsstrahlung amplitude \mathcal{M}_γ (see Fig. 7) must be considered. In the first approach the amplitudes are generated with `FeynArts` and analytically squared within *Mathematica* using `FeynCalc` [78]. We use `MadGraph` [79] and `FormCalc` for internal checks, however, the computational performance of the `FeynArts/FeynCalc`-based code turns out to be more efficient. Alternatively, the corresponding Feynman-diagrams are generated with `QGraf` and the corresponding amplitudes, as well as the squared matrix elements, are evaluated analytically with FORM. In both approaches, the numerical evaluation of the bremsstrahlung contributions is carried out in FORTRAN using the VEGAS [80] algorithm.

In the computation of the real corrections, care has to be taken since the phase-space integral over $|\mathcal{M}_\gamma|^2$ exhibits IR singularities in phase-space regions where the photon is radiated collinear to an initial-state quark or becomes soft, i.e. the energy of the photon goes to zero. We apply the well-known technique of the two-cut-off phase-space slicing to analytically carry out the phase-space integration over the soft and collinear singularities by using small mass regulators m_q and λ for the light quarks and the photon, respectively, and exploiting universal factorization

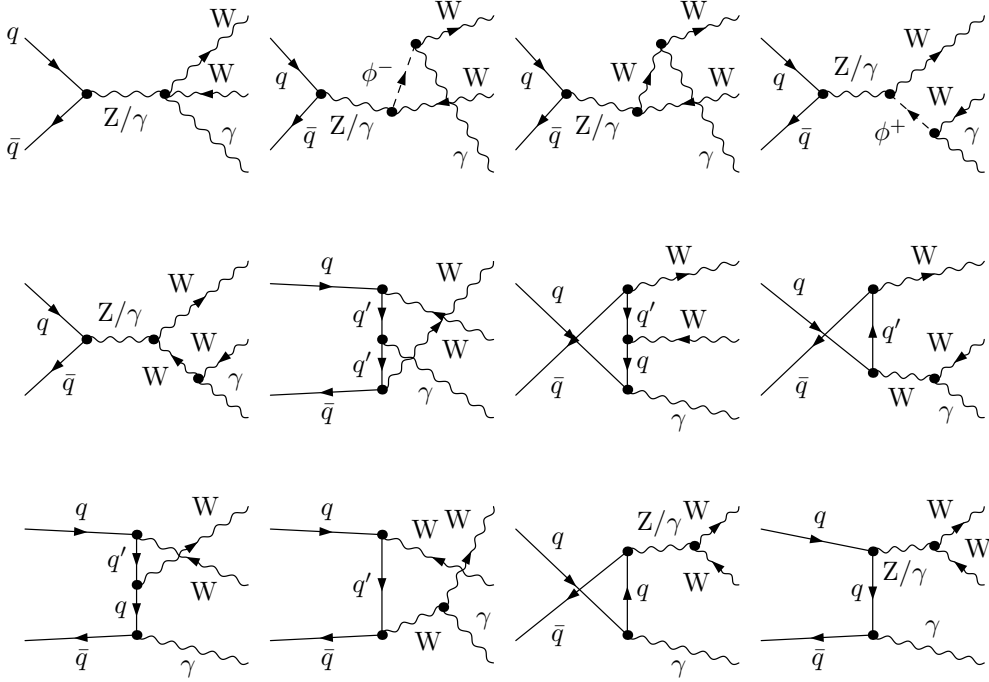


Figure 7: Generic bremsstrahlung diagrams for the process $q\bar{q} \rightarrow W^-W^+\gamma$.

properties for the squared bremsstrahlung amplitudes in the soft and collinear limit (see, e.g., Ref. [81]). Accordingly, the IR singularities appear as $\ln m_q$ and $\ln \lambda$ terms in this particular mass regularisation scheme. Note that the hierarchy $\lambda \ll m_q$ has to be respected carefully in the evaluation of the IR-singular terms. To separate the soft and collinear phase-space configurations from the hard bremsstrahlung, one imposes a cut on the photon energy, $E_\gamma < \Delta E \ll \sqrt{\hat{s}}$ and a cut on the angle between incoming (anti-)quark and photon, $\theta_{q\gamma} < \Delta\theta \ll 1$. The residual phase-space integration corresponding to hard, non-collinear photon emission, i.e. $E_\gamma > \Delta E$ and $\theta_{q\gamma} > \Delta\theta$, can safely be carried out without IR regulators, allowing for an efficient numerical evaluation using **Vegas**. Adding the soft, collinear and hard contributions, the dependence on the slicing parameters ΔE and $\Delta\theta$ cancels out in the computation of IR-safe observables.²

According to the Bloch–Nordsieck theorem [82], the soft singularities emerging from real radiation cancel against corresponding contributions from the virtual corrections related to photon exchange between on-shell legs in loop diagrams. However, the initial-state collinear singularities survive and have to be absorbed in the renormalized PDFs, where we apply the $\overline{\text{MS}}$ factorization scheme as described in Ref. [83]. Since we do not include the leptonic decays of the final-state W bosons in this work, we do not have to deal with subtleties concerning infrared safety arising from the event-selection procedure for photon radiation off charged leptons in the final state.

²Technically, the dimensionless quantity $\delta_s = 2\Delta E/\sqrt{\hat{s}}$ is used as slicing parameter instead of ΔE .

3.3 NLO QCD contributions

In addition to the EW corrections, we have also recalculated the NLO QCD corrections to W-boson pair production, using the same setup as detailed above. The corresponding real corrections exhibit additional partonic channels with one gluon in the initial state, namely

$$qg \rightarrow W^-W^+q, \quad (3.7a)$$

$$g\bar{q} \rightarrow W^-W^+\bar{q}, \quad (3.7b)$$

where the contributions $gb \rightarrow W^-t^* \rightarrow W^-W^+b$ and $g\bar{b} \rightarrow W^+\bar{t}^* \rightarrow W^+W^-\bar{b}$ formally contribute to associated production of a W-boson and a potentially resonant top-quark at leading order and thus have to be treated separately. We exclude those channels from our analysis by discarding events with a b-quark in the final state, assuming a 100% tagging efficiency.

In the numerical analysis one finds that the p_T distribution of the W-boson is plagued by huge NLO QCD K -factors of a few hundreds of percent, resulting in potentially large uncertainties in the theory predictions. To circumvent this problem, we follow the strategy proposed in Ref. [39] and veto events with a hard jet recoiling against a hard W, because these signatures belong to W+jet production at LO rather than being a correction to W-pair production. Technically, we discard events where the transverse momentum of a visible jet (with $p_{T,\text{jet}} > 15$ GeV and $|y_{\text{jet}}| < 2.5$) is larger than half of the highest W-boson p_T . (The important issue of giant QCD K -factors has also been discussed in Ref. [84].)

4 Numerical results

In this section we present numerical results for total cross sections and differential distributions for the process $p\bar{p} \rightarrow W^-W^+ + X$ at the Fermilab Tevatron for a total CM energy of $\sqrt{s} = 1.96$ TeV, as well as for the process $pp \rightarrow W^-W^+ + X$ at the CERN LHC with CM energies of $\sqrt{s} = 8$ TeV (LHC8) and $\sqrt{s} = 14$ TeV (LHC14), respectively. We discuss in detail the phenomenological implications of the EW corrections. In the following the relative corrections δ are defined through $\sigma_{\text{NLO}} = (1+\delta)\sigma_{\text{LO}}$. The photon- and gluon-induced channels (2.2) and (2.3), although formally contributing at leading order, are also considered as relative corrections $\delta_{\gamma\gamma}$ and δ_{gg} , respectively.

4.1 Input parameters and event selection

We use the following SM input parameters for the numerical analysis,

$$\begin{aligned} G_\mu &= 1.16637 \times 10^{-5} \text{ GeV}^{-2}, \\ M_W &= 80.398 \text{ GeV}, & M_Z &= 91.1876 \text{ GeV}, \\ M_H &= 125 \text{ GeV}, & m_t &= 173.4 \text{ GeV}, \end{aligned} \quad (4.1)$$

which are taken from Ref. [85]. In the on-shell scheme applied in our computation, the weak mixing angle $\cos^2\theta_w = M_W^2/M_Z^2$ is a derived quantity. For the computation of the process $q\bar{q} \rightarrow W^-W^+$ and its EW radiative corrections, we use the MSTW2008LO PDF set [86] in the LHAPDF setup [87]. In order to consistently include $\mathcal{O}(\alpha)$ corrections, in particular real radiation with the resulting collinear singularities, PDFs should take in principle these QED effects into account. Such a PDF analysis has been performed in Ref. [66], and the $\mathcal{O}(\alpha)$ effects are known to be small, as far as their effect on the quark distribution is concerned [88]. In addition, the currently available PDFs incorporating $\mathcal{O}(\alpha)$ corrections [66] include QCD effects

at NLO, whereas our EW analysis is LO with respect to perturbative QCD only. For these reasons, the MSTW2008LO set is used as our default choice for the $q\bar{q}$ process.

W-pair production through gluon fusion is considered at leading order, hence the same leading-order set [86] is implemented. For W-pair production through the partonic subprocess $\gamma\gamma \rightarrow W^-W^+$ we use the MRST2004QED set [66]. Note that this set has been also used in Ref. [89] to predict the contamination of the Drell–Yan process by the $\gamma\gamma \rightarrow \mu^+\mu^-$ contribution.

For the computation of the QCD corrections, however, the MSTW2008NLO set is adopted, corresponding to a value of $\alpha_s(M_Z) = 0.1202$. As explained above, the CKM matrix can be assumed to be diagonal. The renormalization and factorization scales are always identified, our default scale choice being the phase-space dependent average of the W-boson transverse masses

$$\mu_R = \mu_F = \overline{m_T} = \frac{1}{2} \left(\sqrt{M_W^2 + p_{T,W^-}^2} + \sqrt{M_W^2 + p_{T,W^+}^2} \right) \quad (4.2)$$

for the evaluation of the QCD as well as the EW corrections.³ A similar scale choice was taken in Ref. [56] for the computation of the EW corrections to four-lepton production at the LHC. In our default setup, we require a minimum transverse momentum and a maximum rapidity for the final-state W bosons,

$$p_{T,W^\pm} > 15 \text{ GeV}, \quad |y_{W^\pm}| < 2.5, \quad (4.3)$$

to exclude events where the bosons are emitted collinear to the initial-state partons. As far as QCD corrections are concerned, the jet veto introduced before is only applied to visible jets with

$$p_{T,\text{jet}} > 15 \text{ GeV}, \quad |y_{\text{jet}}| < 2.5 \quad (4.4)$$

to ensure infrared safety.

4.2 Integrated cross sections

We start the discussion of our numerical results with the presentation of integrated cross sections at the LHC and Tevatron, evaluated with our default setup. Table 1 shows integrated LO cross sections, together with the (relative) EW corrections, contributions from $\gamma\gamma$, gluon fusion and QCD corrections. Moreover, relative corrections due to massive-boson radiation (denoted as δ_{WWV}) are included, which will be discussed in the following chapter. In addition, the corresponding results for the total cross sections without any event-selection cuts and without a dedicated jet veto are shown in Table 2 as a benchmark. While our default cuts reduce the LO $q\bar{q}$ -induced cross section by 44% (34%) at the LHC14 (LHC8), the Tevatron cross section is only marginally affected. The relative EW corrections are changed significantly but remain small as expected. In contrast, the relative QCD corrections to the total cross sections are reduced from $\sim 40\%$ (30%) at the LHC (Tevatron) to almost zero (10%) after introducing the jet veto proposed at the end of Section 4.1.

Predictions for the production cross section with cuts on the transverse momenta or the invariant mass of the W-pair have been presented already in Section 2. For cross checks and to simplify numerical comparisons we show in Tables 3 and 4 the cross sections and the corresponding relative corrections for different cut values on the W transverse momenta (Table 3) and on the invariant mass of the W-boson pair (Table 4). While the relative corrections δ_{gg} due to process (2.3) are negligible at high invariant masses and transverse momenta, we recall that the photon-induced

³Although the relative EW corrections hardly depend on the choice of the factorization scale, the QCD corrections can be significantly stabilized using a scale which is adjusted to the kinematics of the underlying hard process. (For a detailed discussion of this important issue, see, e.g., Ref. [40].)

default cuts	$\sigma_{\text{LO}}^{q\bar{q}}$ (pb)	δ_{EW} (%)	$\delta_{\gamma\gamma}$ (%)	δ_{gg} (%)	$\delta_{\text{QCD}}^{\text{veto}}$ (%)	δ_{WWV} (%)
LHC8	23.99	-0.8	1.7	5.8	1.9	0.3
LHC14	42.39	-0.9	1.7	9.6	0.5	0.4
Tevatron	7.054	-0.6	0.5	0.5	11.4	0.1

Table 1: Integrated leading-order cross sections and relative corrections for the LHC and the Tevatron evaluated with the default setup defined in Section 4.1.

no cuts	$\sigma_{\text{LO}}^{q\bar{q}}$ (pb)	δ_{EW} (%)	$\delta_{\gamma\gamma}$ (%)	δ_{gg} (%)	$\delta_{\text{QCD}}^{\text{full}}$ (%)	δ_{WWV} (%)
LHC8	35.51	-0.4	1.5	5.4	39.5	0.3
LHC14	75.02	-0.5	1.6	8.1	44.2	0.3
Tevatron	7.916	-0.2	0.5	0.5	32.0	0.1

Table 2: Total leading-order cross sections and corresponding relative corrections for the LHC and the Tevatron without any phase-space cuts.

channels lead to surprisingly large relative contributions of $\sim +20\%$ at $M_{\text{WW}} \sim 2$ TeV, compensating a significant part of the moderate negative Sudakov-enhanced genuine EW contributions. This behaviour may be understood qualitatively recalling that the partonic cross section $\hat{\sigma}_{\gamma\gamma}$ is, for sufficiently high energies, given by a constant, $\hat{\sigma}_{\gamma\gamma} = 8\pi\alpha^2/M_{\text{W}}^2 + \mathcal{O}(1/\hat{s})$, and strongly peaked at small angles, while the corresponding cross section $\hat{\sigma}_{q\bar{q}}$ for large \hat{s} decreases as $\ln(\hat{s}/M_{\text{W}}^2)/\hat{s}$. Although the NLO QCD corrections turn out to be accidentally small in our default setup, they still amount to 20% for large $M_{\text{WW}}^{\text{cut}}$ and $p_{\text{T}}^{\text{cut}}$, respectively, exhibiting a similar behaviour at the LHC and the Tevatron (see Figs. 3, 4 and Tables 3, 4).

$p_{\text{T}}^{\text{cut}}$ (GeV)	$\sigma_{\text{LO}}^{q\bar{q}}$ (pb)	δ_{EW} (%)	$\delta_{\gamma\gamma}$ (%)	δ_{gg} (%)	$\delta_{\text{QCD}}^{\text{veto}}$ (%)	δ_{WWV} (%)
50	19.80	-3.0	2.5	9.6	3.5	0.6
100	5.379	-7.1	3.8	9.2	9.0	1.0
250	$35.31 \cdot 10^{-2}$	-18.9	5.8	7.3	16.7	2.3
500	$23.05 \cdot 10^{-3}$	-33.8	7.0	3.7	18.1	4.0
750	$33.04 \cdot 10^{-4}$	-45.0	7.9	2.2	18.6	5.3
1000	$67.04 \cdot 10^{-5}$	-53.9	8.9	1.4	18.6	6.1
1250	$16.39 \cdot 10^{-5}$	-61.4	10.2	1.0	19.5	6.6
1500	$44.79 \cdot 10^{-6}$	-67.8	11.8	0.8	20.4	6.9

Table 3: Integrated leading-order cross sections and relative corrections for different values of $p_{\text{T}}^{\text{cut}}$ at the LHC at $\sqrt{s} = 14$ TeV, evaluated with the default setup defined in Section 4.1.

$M_{\text{WW}}^{\text{cut}}$ (GeV)	$\sigma_{\text{LO}}^{q\bar{q}}$ (pb)	δ_{EW} (%)	$\delta_{\gamma\gamma}$ (%)	δ_{gg} (%)	$\delta_{\text{QCD}}^{\text{veto}}$ (%)	δ_{WWV} (%)
200	28.84	-2.2	2.2	8.9	7.4	0.5
300	9.492	-4.1	3.8	6.4	14.0	0.8
500	1.841	-7.5	7.2	4.8	19.2	1.4
1000	$12.08 \cdot 10^{-2}$	-17.7	14.4	2.6	24.5	3.2
1500	$20.37 \cdot 10^{-3}$	-25.4	18.1	1.4	23.5	4.2
2000	$48.79 \cdot 10^{-4}$	-31.4	21.6	0.9	23.0	4.9
2500	$13.81 \cdot 10^{-4}$	-36.3	25.6	0.6	22.6	5.2
3000	$42.99 \cdot 10^{-5}$	-40.6	30.5	0.4	22.4	5.4

Table 4: Integrated leading-order cross sections and relative corrections for different values of $M_{\text{WW}}^{\text{cut}}$ at the LHC at $\sqrt{s} = 14$ TeV, evaluated with the default setup defined in Section 4.1.

4.3 Transverse-momentum, invariant-mass and rapidity distributions

In a first step we show the transverse-momentum distributions of W^- and W^+ (Fig. 8) and the distributions of the invariant mass M_{WW} (Figure 9) for LHC14, LHC8 and the Tevatron. The interpretation of the results is similar to that of the partially integrated cross sections presented in Figs. 3 and 4 in Section 2. In particular, we again observe the large Sudakov logarithms resulting in corrections of -30% for p_{T} values around 800 GeV. Again, the correction for the invariant-mass distribution is smaller, since large M_{WW} may still involve small momentum transfer \hat{t} . At the LHC, the QCD corrections evaluated with the jet veto proposed in Section 4.1 still reach 50% (20%) at high p_{T} (M_{WW}), while at the Tevatron they do not exceed 20% even at large transverse momenta.

Rapidity distributions of W^+ and W^- individually are shown in Fig. 10. Note that the rapidity distributions of W^+ and W^- are different at the LHC, as a consequence of the asymmetric piece of the differential cross section for $u\bar{u} \rightarrow W^-W^+$ and $d\bar{d} \rightarrow W^-W^+$, and the difference between valence- and sea-quark distributions. For the Tevatron one finds $d\sigma_{W^+}(y) = d\sigma_{W^-}(-y)$. At the LHC8 (LHC14), gluon fusion and the $\gamma\gamma$ process increase the W -pair production rate by $\sim 5\%$ (10%) and $\sim 2\%$ (2%), respectively. The EW corrections are $\sim -1\%$, reflecting the small \hat{s} of typical events and the absence of the large negative Sudakov logarithms. At the Tevatron, only QCD corrections must be considered for this particular observable; EW corrections, $\gamma\gamma$ and gg fusion can safely be neglected.

The rapidity distributions for the LHC14 and the LHC8 for the subsamples with invariant mass $M_{\text{WW}} > 500$ GeV and $M_{\text{WW}} > 1000$ GeV are shown in Figs. 11 and 12, respectively. In these cases EW corrections and the $\gamma\gamma$ process are significantly more important.

Let us finally consider W -pair production at the highest energies accessible at the LHC. As already mentioned in Section 2, the distribution in the rapidity difference (for fixed M_{WW}) between W^+ and W^- bosons can be directly related to the angular distribution in the WW rest frame and thus can be used to search for anomalous couplings at the TeV scale. In Figs. 13 and 14 we therefore show these distributions for $M_{\text{WW}} > 1.5$ TeV for LHC14 and $M_{\text{WW}} > 0.75$ TeV for LHC8, respectively. At the LHC14, large contributions are visible both from the $\gamma\gamma$ process ($+60\%$) and from the weak corrections (-45%), leading to a strong distortion of this particular

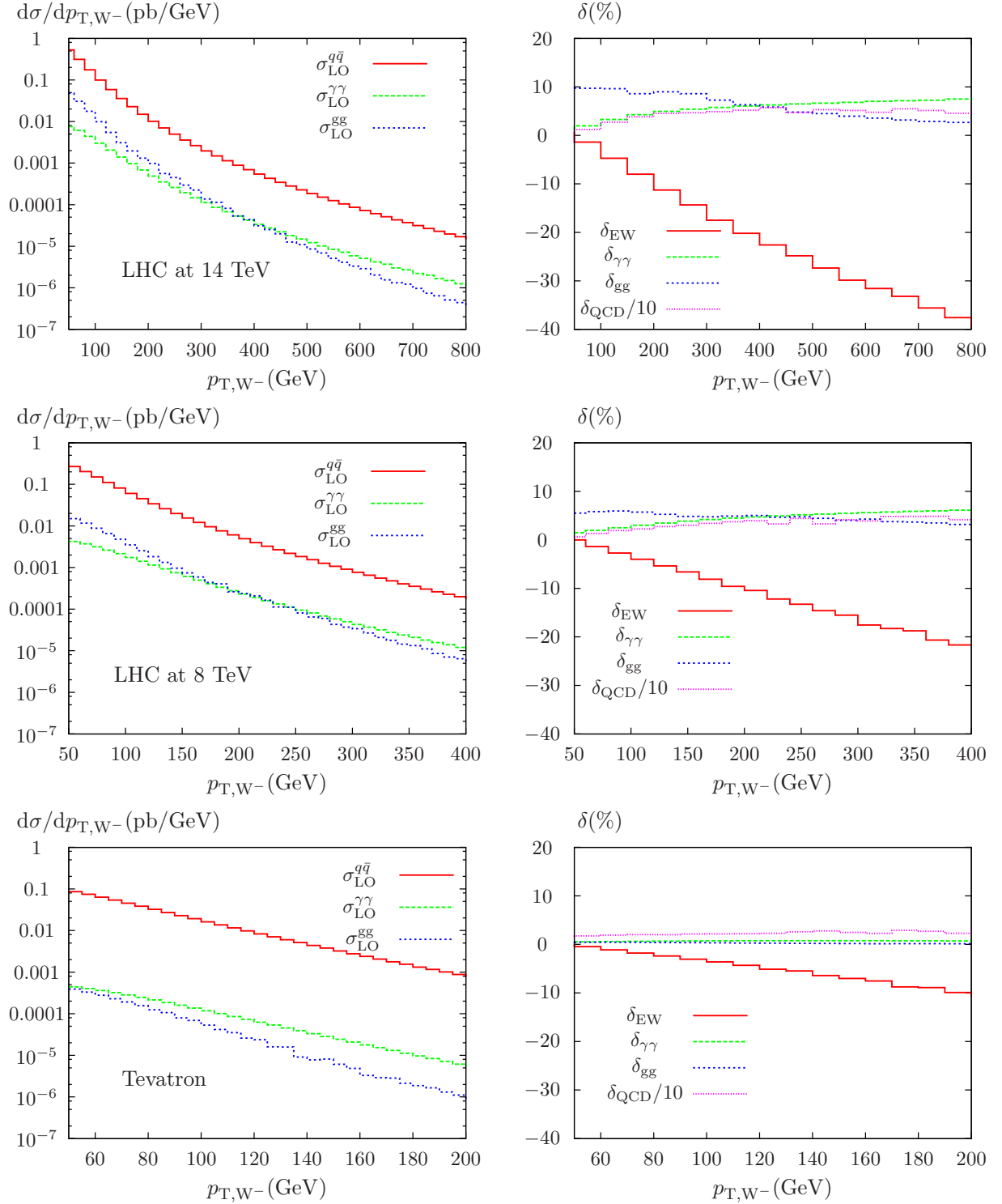


Figure 8: Distributions of the W^- transverse momentum at the LHC14 (top), LHC8 (center) and the Tevatron (bottom). On the left-hand side, LO contributions due to processes (2.1)($q\bar{q}$), (2.2)($\gamma\gamma$), and (2.3)(gg) are shown. On the right-hand side, corresponding relative corrections are presented, normalized to the dominating LO channel (2.1). See text for details.

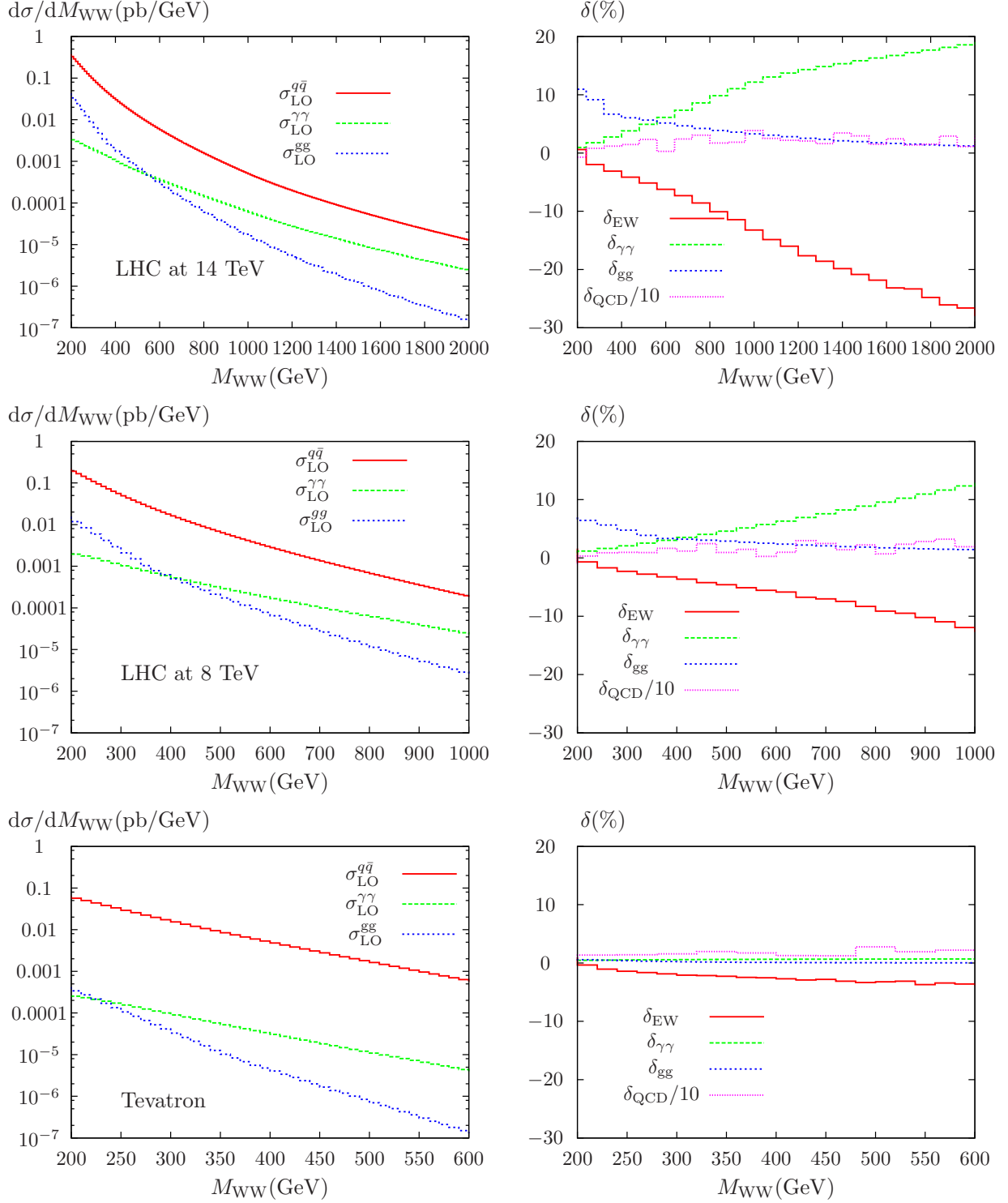


Figure 9: Distributions of the invariant mass of the W-boson pair at the LHC14 (top), LHC8 (center) and the Tevatron (bottom). On the left-hand side, LO contributions due to processes (2.1)($q\bar{q}$), (2.2)($\gamma\gamma$), and (2.3)(gg) are shown. On the right-hand side, corresponding relative corrections are presented, normalized to the dominating LO channel (2.1). See text for details.

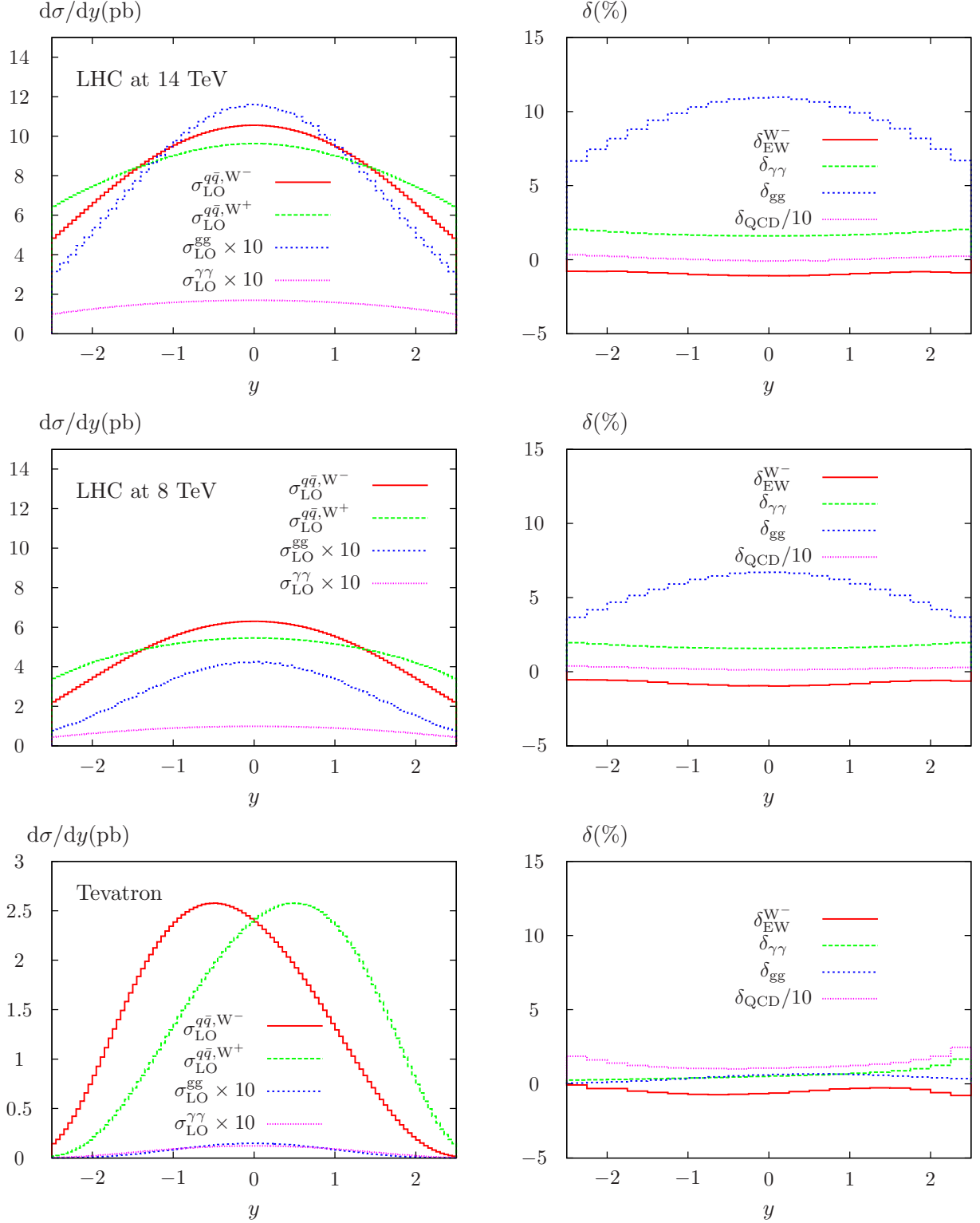


Figure 10: Distributions of the rapidities of the W-bosons at the LHC14 (top), LHC8 (center) and the Tevatron (bottom). On the left-hand side, LO contributions due to processes (2.1)($q\bar{q}$), (2.2)($\gamma\gamma$), and (2.3)(gg) are shown. On the right-hand side, corresponding relative corrections are presented, normalized to the dominating LO channel (2.1). See text for details.

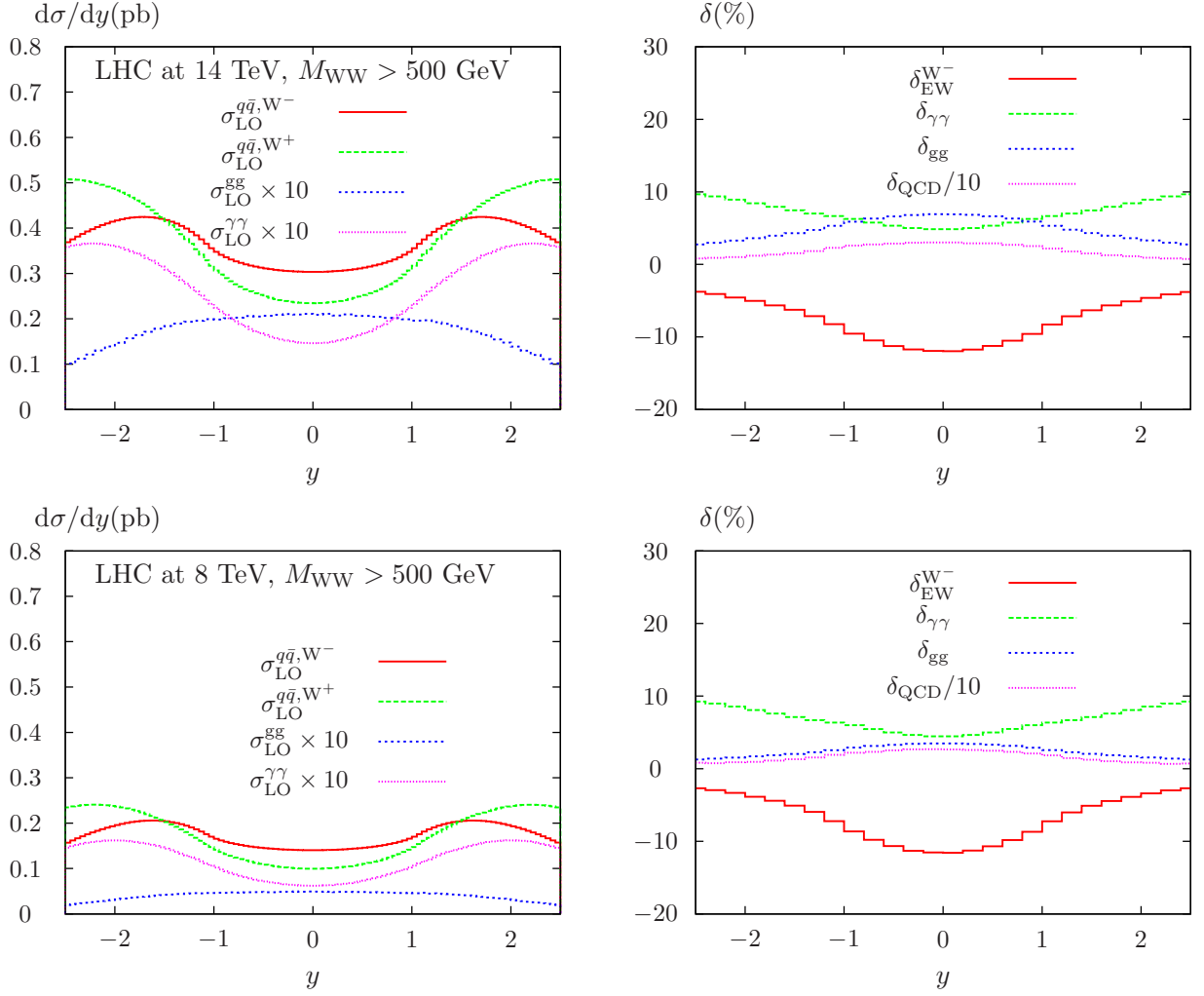


Figure 11: Distributions of the rapidities of the W-bosons at the LHC14 (top) and LHC8 (bottom) for $M_{WW} > 500$ GeV. On the left-hand side, LO contributions due to processes (2.1)($q\bar{q}$), (2.2)($\gamma\gamma$), and (2.3)(gg) are shown. On the right-hand side, corresponding relative corrections are presented, normalized to the dominating LO channel (2.1). See text for details.

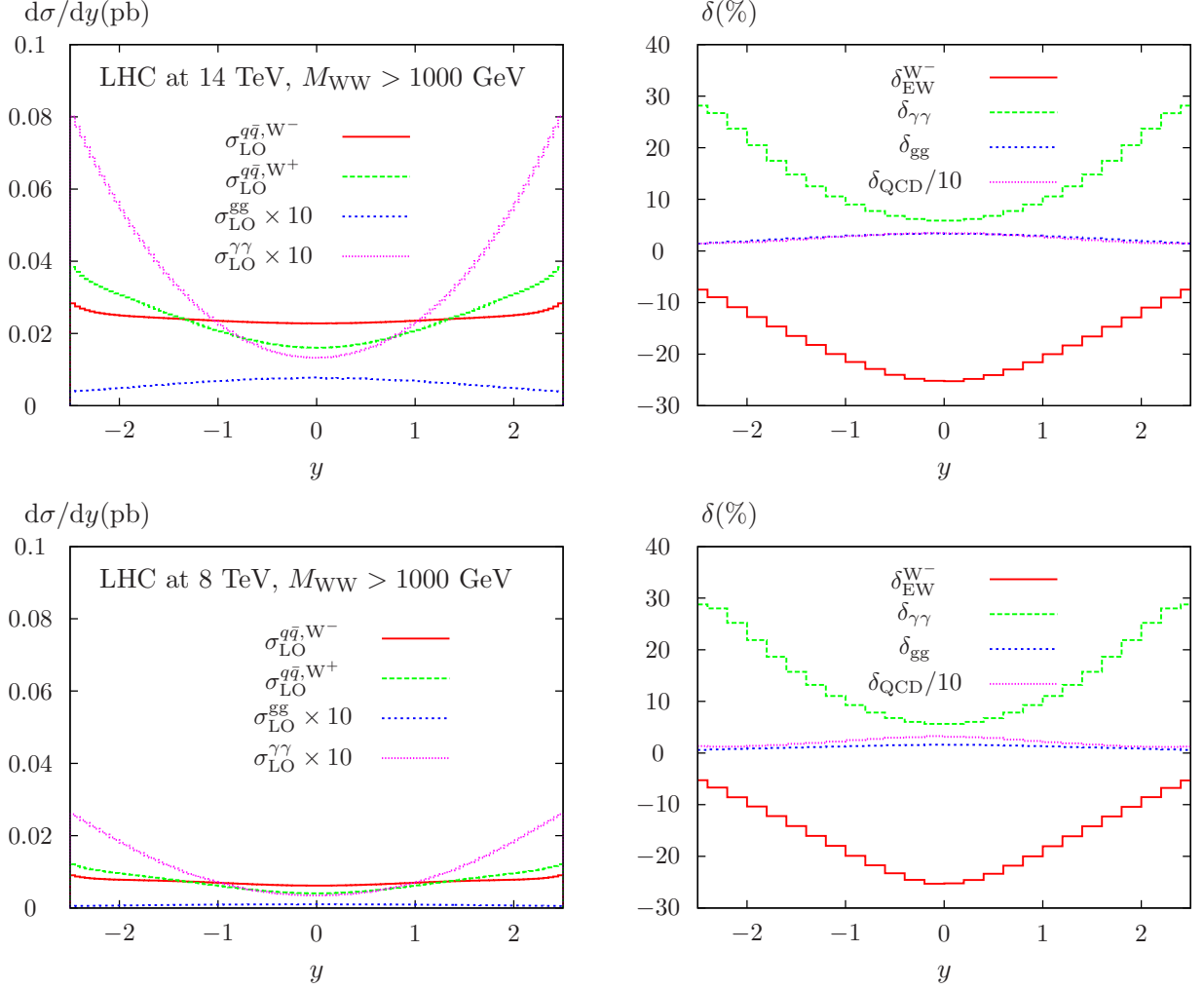


Figure 12: Distributions of the rapidities of the W-bosons at the LHC14 (top) and LHC8 (bottom) for $M_{WW} > 1000$ GeV. On the left-hand side, LO contributions due to processes (2.1)($q\bar{q}$), (2.2)($\gamma\gamma$), and (2.3)(gg) are shown. On the right-hand side, corresponding relative corrections are presented, normalized to the dominating LO channel (2.1). See text for details.

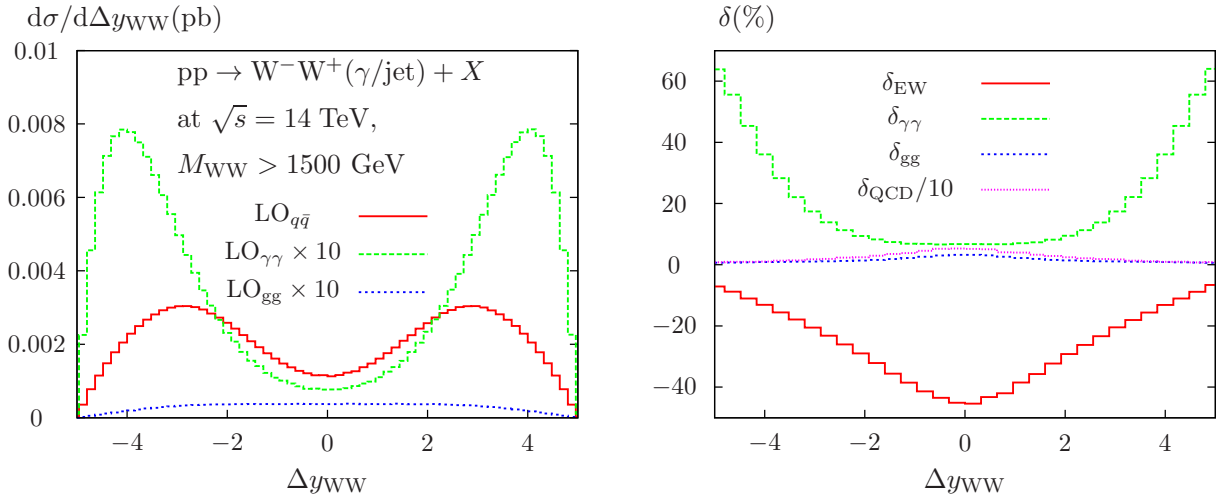


Figure 13: Distributions of the W-boson rapidity gap at the LHC14 for $M_{WW} > 1500$ GeV. On the left-hand side, LO contributions due to processes (2.1)($q\bar{q}$), (2.2)($\gamma\gamma$), and (2.3)(gg) are shown. On the right-hand side, corresponding relative corrections are presented, normalized to the dominating LO channel (2.1). See text for details.

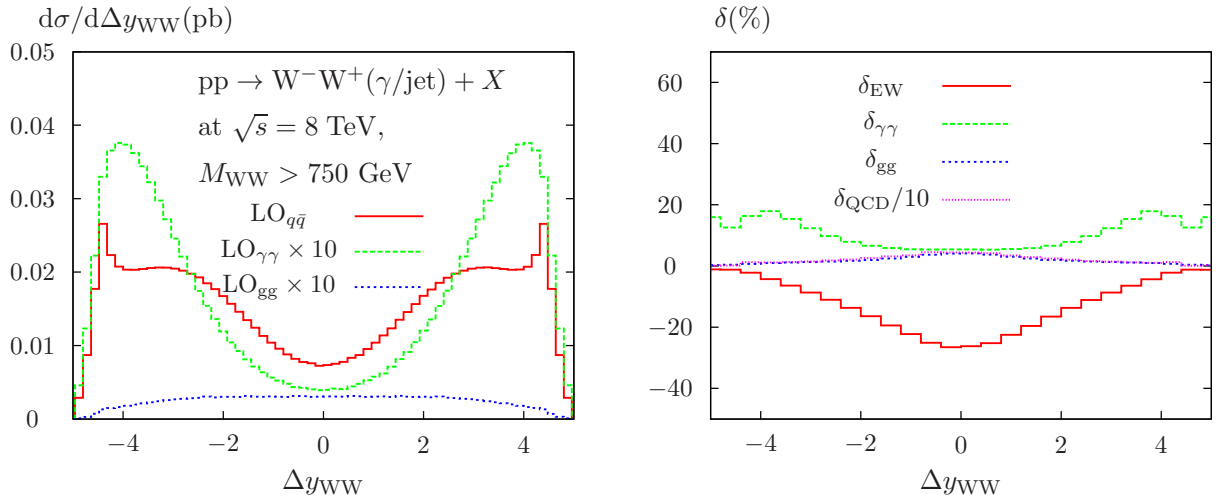


Figure 14: Distributions of the W-boson rapidity gap at the LHC8 for $M_{WW} > 750$ GeV. On the left-hand side, LO contributions due to processes (2.1)($q\bar{q}$), (2.2)($\gamma\gamma$), and (2.3)(gg) are shown. On the right-hand side, corresponding relative corrections are presented, normalized to the dominating LO channel (2.1). See text for details.

distribution. As already discussed in Section 2, the additional contributions from gg and $\gamma\gamma$ fusion are small in the region accessible to the Tevatron and hence will not be discussed further.

Finally, we compare our predictions to older results obtained in the high-energy approximation. Unfortunately, a tuned comparison of our results with the ones presented in Ref. [56] is not possible, since in that paper dedicated event-selection cuts on the leptonic decay products of the W bosons are applied. However, comparing Fig. 7 (bottom, left) from Ref. [56] with Fig. 5 (bottom, right), we find a reasonable agreement for the relative EW corrections within a few percent. Here, we assume that each of the charged leptons on average carries away 50% of the momentum of the decaying W , and a strong correlation between Δy_{WW} and $\Delta y_{l\bar{l}}$, which seems to be justified in case of strongly-boosted W s.

5 Radiation of massive vector bosons

Finally, we discuss the phenomenological effects of additional massive vector bosons in the final state produced in the partonic processes

$$u_i \bar{d}_j \rightarrow W^- W^+ W^+, \quad (5.1)$$

$$\bar{u}_i d_j \rightarrow W^- W^+ W^-, \quad (5.2)$$

$$q\bar{q} \rightarrow W^- W^+ Z. \quad (5.3)$$

Although these channels are parametrically suppressed by one order of the EW coupling, collinear or soft massive boson radiation may potentially lead to logarithmically enhanced contributions and thus needs further investigation. In the numerical analysis we use a simplified approach to conservatively estimate the pollution of W -pair production which can be expected from 3-boson final states; we treat the additional boson completely inclusively, whereas our default cuts are applied to those opposite-sign W -bosons with highest p_T . In Fig. 15 we present the corresponding numerical results for the WWV ($V = W, Z$) final state as well as the contribution from hard-photon radiation ($p_{T,\gamma} > 15$ GeV, $|y_\gamma| < 2.5$) relative to quark-induced WW production at leading order. (The corresponding numbers can be found in Tables 3 and 4, respectively.) The relative corrections due to massive boson radiation are below 5% even for large transverse momenta and invariant masses and therefore of minor importance. Remarkably enough the contribution from hard photon radiation with these cuts (which is included in the cross sections discussed in the previous chapter) is numerically close to the one from additional massive boson radiation.

6 Conclusions

We have calculated the full NLO EW corrections to W -boson pair production at hadron colliders and present predictions valid in the full energy reach of the LHC. At large parton CM energies, the relative corrections are dominated by the well-known universal Sudakov logarithms that lead to substantial negative contributions, while the QCD corrections turn out to be moderate after application of a dynamic jet veto.

As a surprising new result we find that photon-induced contributions can be of the same size as the genuine EW corrections at high energies and moderate scattering angles and thus must not be neglected when predicting W -boson pair production at highest energies. At low scattering angles, however, the $\gamma\gamma$ channel dominates the EW contributions at $\mathcal{O}(\alpha^3)$ even at moderate energies. In the future, the leptonic decays of the W bosons should be included

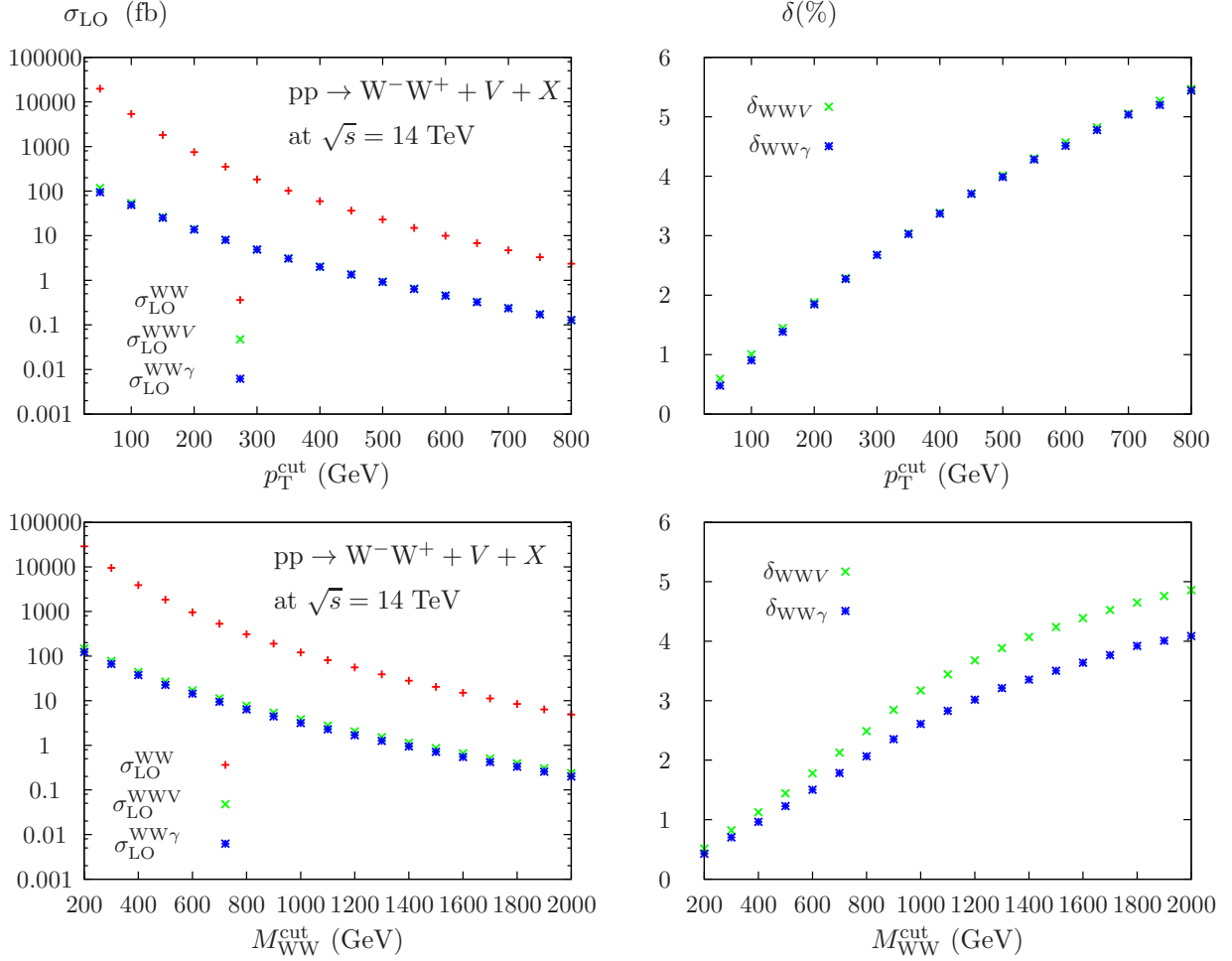


Figure 15: Left: Total LO cross sections for WW, WWV ($V = W, Z$) and WW γ production; Right: Corrections due to WWV and WW γ relative to quark-induced W-pair production. See text for details.

properly, allowing for a realistic event definition to match the increasing accuracy of future LHC measurements.

Acknowledgements

We would like to thank Peter Marquard for fruitful discussions. This work has been supported by “Strukturiertes Promotionskolleg Elementarteilchen- und Astroteilchenphysik”, SFB TR9 “Computational and Particle Physics” and BMBF Contract 05HT4VKATI3.

References

- [1] S. Chatrchyan *et al.* [CMS Collaboration], Phys. Lett. B **704** (2011) 123 [arXiv:1107.4771 [hep-ex]].
- [2] G. Aad *et al.* [ATLAS Collaboration], arXiv:1112.6297 [hep-ex].

- [3] D. A. Ross and M. J. G. Veltman, Nucl. Phys. B **95** (1975) 135.
- [4] J. H. Kühn and A. A. Penin, hep-ph/9906545.
- [5] V. S. Fadin, L. N. Lipatov, A. D. Martin and M. Melles, Phys. Rev. D **61** (2000) 094002 [hep-ph/9910338].
- [6] M. Ciafaloni, P. Ciafaloni and D. Comelli, Phys. Rev. Lett. **84** (2000) 4810 [hep-ph/0001142].
- [7] J. H. Kühn, A. A. Penin and V. A. Smirnov, Eur. Phys. J. C **17** (2000) 97 [hep-ph/9912503].
- [8] M. Melles, Phys. Rev. D **63** (2001) 034003 [hep-ph/0004056].
- [9] M. Melles, Phys. Rev. D **64** (2001) 014011 [hep-ph/0012157].
- [10] A. Denner, M. Melles and S. Pozzorini, Nucl. Phys. B **662** (2003) 299 [hep-ph/0301241].
- [11] J. H. Kühn, S. Moch, A. A. Penin and V. A. Smirnov, Nucl. Phys. B **616** (2001) 286 [Erratum-ibid. B **648** (2003) 455] [hep-ph/0106298].
- [12] B. Feucht, J. H. Kühn, A. A. Penin, V. A. Smirnov, and , Phys. Rev. Lett. **93** (2004) 101802 [hep-ph/0404082].
- [13] B. Jantzen, J. H. Kühn, A. A. Penin, V. A. Smirnov, and , Phys. Rev. D **72** (2005) 051301 [Erratum-ibid. D **74** (2006) 019901] [hep-ph/0504111].
- [14] B. Jantzen, V. A. Smirnov and , Eur. Phys. J. C **47** (2006) 671 [hep-ph/0603133].
- [15] B. Jantzen, J. H. Kühn, A. A. Penin, V. A. Smirnov and , Nucl. Phys. B **731** (2005) 188 [Erratum-ibid. B **752** (2006) 327] [hep-ph/0509157].
- [16] A. Denner and S. Pozzorini, Eur. Phys. J. C **18** (2001) 461 [hep-ph/0010201]; A. Denner and S. Pozzorini, Eur. Phys. J. C **21** (2001) 63 [hep-ph/0104127]; S. Pozzorini, Nucl. Phys. B **692** (2004) 135 [hep-ph/0401087].
- [17] J. -y. Chiu, A. Fuhrer, A. H. Hoang, R. Kelley and A. V. Manohar, Phys. Rev. D **79** (2009) 053007 [arXiv:0901.1332 [hep-ph]].
- [18] V. N. Gribov, Sov. J. Nucl. Phys. **5** (1967) 280 [Yad. Fiz. **5** (1967) 399].
- [19] V. N. Gribov, L. N. Lipatov and G. V. Frolov, Sov. J. Nucl. Phys. **12** (1971) 543 [Yad. Fiz. **12** (1970) 994].
- [20] L. N. Lipatov, Nucl. Phys. B **307** (1988) 705.
- [21] V. Del Duca, Nucl. Phys. B **345** (1990) 369.
- [22] J. H. Kühn, F. Metzler and A. A. Penin, Nucl. Phys. B **795** (2008) 277 [Erratum-ibid. **818** (2009) 135] [arXiv:0709.4055 [hep-ph]].
- [23] J. H. Kühn, F. Metzler, A. A. Penin and S. Uccirati, JHEP **1106** (2011) 143 [arXiv:1101.2563 [hep-ph]].
- [24] A. Fuhrer, A. V. Manohar, J. -y. Chiu and R. Kelley, Phys. Rev. D **81** (2010) 093005 [arXiv:1003.0025 [hep-ph]].

- [25] J. H. Kühn, A. Scharf and P. Uwer, Eur. Phys. J. C **45** (2006) 139 [hep-ph/0508092].
- [26] J. H. Kühn, A. Scharf and P. Uwer, Eur. Phys. J. C **51** (2007) 37 [hep-ph/0610335].
- [27] W. Bernreuther, M. Fuecker and Z. -G. Si, Phys. Rev. D **74** (2006) 113005 [hep-ph/0610334].
- [28] W. Bernreuther, M. Fuecker and Z. G. Si, Phys. Lett. B **633** (2006) 54 [hep-ph/0508091].
- [29] S. Moretti, M. R. Nolten and D. A. Ross, Phys. Lett. B **639** (2006) 513 [Erratum-ibid. B **660** (2008) 607] [hep-ph/0603083].
- [30] W. Beenakker, A. Denner, W. Hollik, R. Mertig, T. Sack and D. Wackerroth, Nucl. Phys. B **411** (1994) 343.
- [31] C. Kao and D. Wackerroth, Phys. Rev. D **61** (2000) 055009 [hep-ph/9902202].
- [32] J. H. Kühn, A. Scharf and P. Uwer, Phys. Rev. D **82** (2010) 013007 [arXiv:0909.0059 [hep-ph]].
- [33] J. H. Kühn, A. Kulesza, S. Pozzorini and M. Schulze, Phys. Lett. B **609** (2005) 277 [hep-ph/0408308].
- [34] J. H. Kühn, A. Kulesza, S. Pozzorini and M. Schulze, Nucl. Phys. B **727** (2005) 368 [hep-ph/0507178].
- [35] J. H. Kühn, A. Kulesza, S. Pozzorini and M. Schulze, JHEP **0603** (2006) 059 [hep-ph/0508253].
- [36] J. H. Kühn, A. Kulesza, S. Pozzorini and M. Schulze, Phys. Lett. B **651** (2007) 160 [hep-ph/0703283 [HEP-PH]].
- [37] J. H. Kühn, A. Kulesza, S. Pozzorini and M. Schulze, Nucl. Phys. B **797** (2008) 27 [arXiv:0708.0476 [hep-ph]].
- [38] W. Hollik, T. Kasprzik and B. A. Kniehl, Nucl. Phys. B **790** (2008) 138 [arXiv:0707.2553 [hep-ph]].
- [39] A. Denner, S. Dittmaier, T. Kasprzik and A. Mück, JHEP **0908** (2009) 075 [arXiv:0906.1656 [hep-ph]].
- [40] A. Denner, S. Dittmaier, T. Kasprzik and A. Mück, JHEP **1106** (2011) 069 [arXiv:1103.0914 [hep-ph]].
- [41] J. Ohnemus, Phys. Rev. **D44** (1991) 3477-3489.
- [42] S. Frixione, Nucl. Phys. **B410** (1993) 280-324.
- [43] J. Ohnemus, Phys. Rev. **D51** (1995) 1068-1076. [hep-ph/9407370].
- [44] J. Ohnemus, Phys. Rev. **D50** (1994) 1931-1945. [arXiv:hep-ph/9403331 [hep-ph]].
- [45] L. J. Dixon, Z. Kunszt, A. Signer, Nucl. Phys. **B531** (1998) 3-23. [hep-ph/9803250].
- [46] L. J. Dixon, Z. Kunszt, A. Signer, Phys. Rev. **D60** (1999) 114037. [hep-ph/9907305].
- [47] D. De Florian, A. Signer, Eur. Phys. J. **C16** (2000) 105-114. [hep-ph/0002138].

- [48] J. M. Campbell, R. K. Ellis, Phys. Rev. **D60** (1999) 113006. [hep-ph/9905386].
- [49] J. M. Campbell, R. K. Ellis, C. Williams, [arXiv:1105.0020 [hep-ph]].
- [50] S. Frixione, B. R. Webber, [hep-ph/0601192].
- [51] E. W. N. Glover, J. J. van der Bij, Nucl. Phys. **B321** (1989) 561.
- [52] C. Kao, D. A. Dicus, Phys. Rev. **D43** (1991) 1555-1559.
- [53] M. Duhrssen, K. Jakobs, J. J. van der Bij, P. Marquard, JHEP **0505** (2005) 064. [hep-ph/0504006].
- [54] T. Binoth, M. Ciccolini, N. Kauer, M. Krämer, JHEP **0612** (2006) 046. [hep-ph/0611170].
- [55] E. Accomando, A. Denner and S. Pozzorini, Phys. Rev. D **65** (2002) 073003 [hep-ph/0110114].
- [56] E. Accomando, A. Denner and A. Kaiser, Nucl. Phys. B **706** (2005) 325 [hep-ph/0409247].
- [57] E. Accomando, A. Denner, C. Meier, Eur. Phys. J. **C47** (2006) 125-146. [hep-ph/0509234].
- [58] M. Lemoine and M. J. G. Veltman, Nucl. Phys. B **164** (1980) 445.
- [59] M. Böhm, A. Denner, T. Sack, W. Beenakker, F. A. Berends and H. Kuijf, Nucl. Phys. B **304** (1988) 463.
- [60] J. Fleischer, F. Jegerlehner and M. Zralek, BI-TP-88/03.
- [61] W. Beenakker, A. Denner, S. Dittmaier, R. Mertig and T. Sack, Nucl. Phys. B **410** (1993) 245.
- [62] W. Beenakker, F. A. Berends and A. P. Chapovsky, In *Barcelona 1998, Radiative corrections: Application of quantum field theory to phenomenology* 528-536 [hep-ph/9902333].
- [63] S. Jadach, W. Placzek, M. Skrzypek, B. F. L. Ward and Z. Was, Comput. Phys. Commun. **140** (2001) 475 [hep-ph/0104049].
- [64] A. Denner, S. Dittmaier, M. Roth and D. Wackerroth, Nucl. Phys. B **587** (2000) 67 [hep-ph/0006307]; A. Denner, S. Dittmaier, M. Roth and D. Wackerroth, Comput. Phys. Commun. **153** (2003) 462 [hep-ph/0209330].
- [65] A. Denner, S. Dittmaier, M. Roth and L. H. Wieders, Phys. Lett. B **612** (2005) 223 [Erratum-ibid. B **704** (2011) 667] [hep-ph/0502063]; A. Denner, S. Dittmaier, M. Roth and L. H. Wieders, Nucl. Phys. B **724** (2005) 247 [Erratum-ibid. B **854** (2012) 504] [hep-ph/0505042].
- [66] A. D. Martin, R. G. Roberts, W. J. Stirling, R. S. Thorne, Eur. Phys. J. **C39** (2005) 155-161. [hep-ph/0411040].
- [67] E. Accomando and A. Kaiser, Phys. Rev. D **73** (2006) 093006 [hep-ph/0511088].
- [68] J. Küblbeck, M. Böhm and A. Denner, Comput. Phys. Commun. **60** (1990) 165; H. Eck and J. Küblbeck, *Guide to FeynArts 1.0*, University of Würzburg, 1992.
- [69] T. Hahn, Comput. Phys. Commun. **140** (2001) 418 [hep-ph/0012260].

- [70] T. Hahn and M. Pérez-Victoria, *Comput. Phys. Commun.* **118** (1999) 153 [hep-ph/9807565].
- [71] T. Hahn, C. Schappacher, *Comput. Phys. Commun.* **143** (2002) 54-68. [hep-ph/0105349].
- [72] Nogueira, P. Automatic Feynman graph generation. *J. Comput. Phys.*, **vol. 105 (1993)** pp. 279–289.
- [73] Vermaseren, J.A.M. New features of FORM. (2000).
- [74] G. Passarino, M. J. G. Veltman, *Nucl. Phys.* **B160** (1979) 151.
- [75] G. J. van Oldenborgh, J. A. M. Vermaseren, *Z. Phys.* **C46** (1990) 425-438.
- [76] A. Denner, *Fortsch. Phys.* **41** (1993) 307-420. [arXiv:0709.1075 [hep-ph]].
- [77] S. Dittmaier, M. Krämer, *Phys. Rev.* **D65** (2002) 073007. [hep-ph/0109062].
- [78] R. Mertig, M. Böhm and A. Denner, *Comput. Phys. Commun.* **64** (1991) 345.
- [79] J. Alwall *et al.*, *JHEP* **0709** (2007) 028. [arXiv:0706.2334 [hep-ph]].
- [80] G. P. Lepage, *J. Comput. Phys.* **27** (1978) 192 and CLNS-80/447.
- [81] S. Dittmaier, *Nucl. Phys. B* **565** (2000) 69 [hep-ph/9904440].
- [82] F. Bloch, A. Nordsieck, *Phys. Rev.* **52** (1937) 54-59.
- [83] K. P. O. Diener, S. Dittmaier and W. Hollik, *Phys. Rev. D* **69** (2004) 073005 [hep-ph/0310364].
- [84] M. Rubin, G. P. Salam and S. Sapeta, *JHEP* **1009** (2010) 084 [arXiv:1006.2144 [hep-ph]].
- [85] C. Amsler *et al.* [Particle Data Group], *Phys. Lett. B* **667** (2008) 1.
- [86] A. D. Martin *et al.*, *Eur. Phys. J.* **C63**, (2009) 189-285. [arXiv:0901.0002 [hep-ph]].
- [87] M. R. Whalley, D. Bourilkov and R. C. Group, in *HERA and the LHC*, eds. A. de Roeck and H. Jung (CERN-2005-014, Geneva, 2005), p. 575, hep-ph/0508110.
- [88] M. Roth and S. Weinzierl, *Phys. Lett. B* **590** (2004) 190 [hep-ph/0403200].
- [89] S. Dittmaier and M. Huber, *JHEP* **1001** (2010) 060 [arXiv:0911.2329 [hep-ph]].